

Model Development and Experimental Validation of the Fusible Heat Sink Design for Exploration Vehicles

Thomas J. Cognata¹

ESCG/MEI Technologies, Houston, TX, 77058

Thomas Leimkuehler²

Paragon SDC, Houston, TX, 770__

Rubik Sheth³

NASA Johnson Space Center, Houston, TX, 770__

and

Hung Le⁴

ESCG/Geo Control Systems, Houston, TX, 77058

The Fusible Heat Sink is a novel vehicle heat rejection technology which combines a flow through radiator with a phase change material. The combined technologies create a multi-function device able to shield crew members against Solar Particle Events (SPE), reduce radiator extent by permitting sizing to the average vehicle heat load rather than to the peak vehicle heat load, and to substantially absorb heat load excursions from the average while constantly maintaining thermal control system setpoints. This multi-function technology provides great flexibility for mission planning, making it possible to operate a vehicle in hot or cold environments and under high or low heat load conditions for extended periods of time.

This paper describes the modeling and experimental validation of the Fusible Heat Sink technology. The model developed was intended to meet the radiation and heat rejection requirements of a nominal MMSEV mission. Development parameters and results, including sizing and model performance will be discussed. From this flight-sized model, a scaled test-article design was modeled, designed, and fabricated for experimental validation of the technology at Johnson Space Center thermal vacuum chamber facilities. Testing showed performance comparable to the model at nominal loads and the capability to maintain heat loads substantially greater than nominal for extended periods of time.

Nomenclature

T_{xxx}	=	Surface temperature measurement location
FTC_x	=	Frame temperature measurement location
PCM	=	Phase Change Material
$MMSEV$	=	Multi-Mission Space Exploration Vehicle
SPE	=	Solar Particle Event
$IRIP$	=	Integrated Radiator Ice PCM
$LN2$	=	Liquid Nitrogen
Q_x	=	X case of heat rejection from the radiator

I. Introduction

NASA is currently investigating the use of a Multi-Mission Space Exploration Vehicle (MMSEV), with both surface and in-space versions, as shown in Figure 1. A layer of water in the ceiling and/or walls of the vehicle

¹ Sr. Engineer, 2224 Bay Area Blvd, AIAA Member.

² Sr. Aerospace Engineer, Address/Mail Stop, and AIAA Member Grade for third author.

³ Insert Job Title, Address/Mail Stop, and AIAA Member Grade for fourth author (etc).

⁴ Insert Job Title, 2224 Bay Area Blvd, and AIAA Member Grade for fourth author (etc).



Figure 1. Surface and in-space versions of the MMSEV.

is envisioned to provide radiation shielding for the crew members. This water can be frozen and used as a phase change material (PCM) as part of the thermal control system. Integrating this ice PCM with a radiator for heat rejection can reduce the size requirements of the radiator.

The test described herein is the next in a series of increasing fidelity tests. Previous work has examined proof of concept, material and geometry dependence, and predictive model validation. Three years ago^{0,0}, small test articles were tested in a thermal vacuum chamber to examine heat input and removal from different sides of the PCM. A heater supplied heat to the bottom of the PCM while heat was removed from the top radiator surfaces of the test articles. Two years ago^{0,0}, laboratory testing was conducted with a number of interstitial materials, thicknesses, and spacing to provide data for validating thermal models and optimizing the interstitial material. A heater again supplied heat to the bottom of the PCM while heat was removed through a chilled fluid loop and a coldplate attached to the lid of the test articles. In the present test, the investigation returns to a proof of concept thermal vacuum test with a more flight-like test article, the Integrated Radiator Ice PCM (IRIP) otherwise known as the Fusible Heat Sink. Heat is supplied to the PCM by a pumped fluid loop flowing through a coldplate integrated into the test article and heat is removed by radiation from a radiator surface. The test article is much larger than the test articles from previous years, representing one of a set of panels, and is braze-fabricated as one-piece. The test is meant to demonstrate the thermal functionality and evaluate the performance of the IRIP in an appropriate simulated thermal environment.

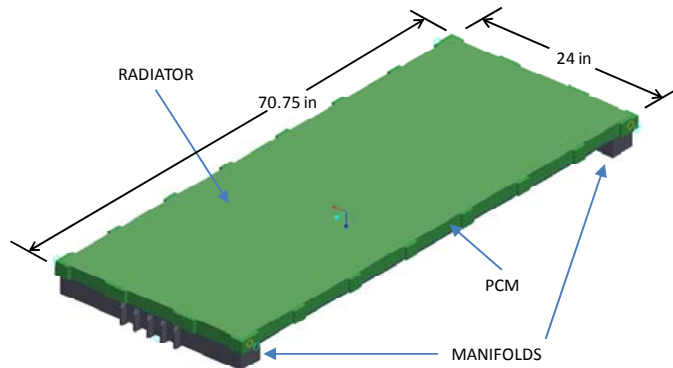


Figure 2. Top view of IRIP.

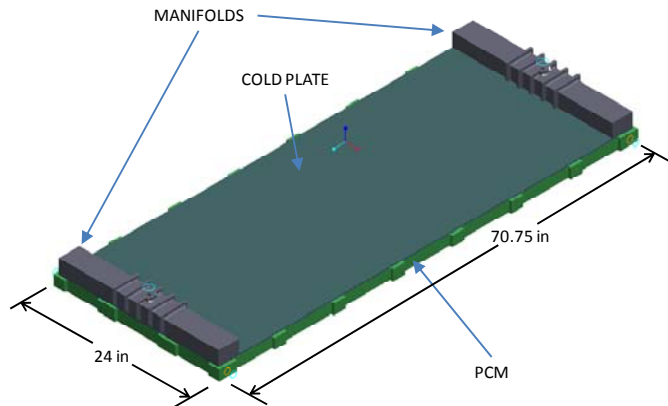


Figure 3. Bottom view of IRIP.

II. Test Setup

Testing was performed in the JSC building 33 vacuum chamber E. Chamber E is a high vacuum chamber with LN2 cooled shrouds to simulate the sink temperature of space.

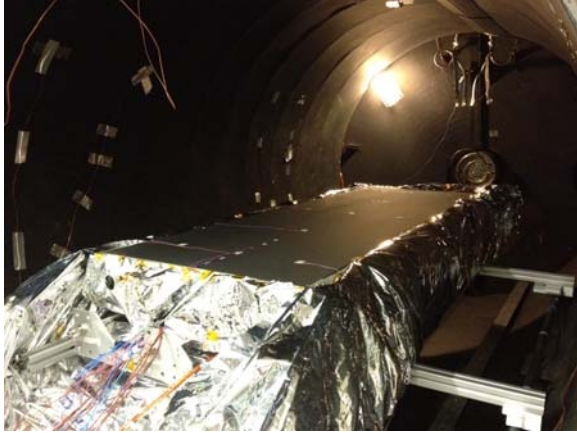


Figure 4. Photo of IRIP in Chamber E with insulation.

The test was performed over a period of 5 days. The IRIP has dimensions of 70.75" x 24" x 4.9". Figure 2 shows the radiator surface and manifolds in a top view of the IRIP, while Figure 3 shows the integrated coldplate fed by manifolds on the bottom of the PCM. The top radiator surface was painted with Lord Corporation's Aeroglaze Z306 and its emissivity was measured to be 0.91. The IRIP was manufactured by Riverside Machine and Engineering. Figure 4 shows the IRIP in Chamber E with Mylar insulation.

Thermocouples are placed on both the top radiator surface and bottom coldplate surface as shown in Figure 5. Both views in the figure are considered a top view. The thermocouple locations for the coldplate are as viewed through the test article from above. Locations T100 through T104 are monitored by the IRIP data acquisition system. All other locations are recorded by a separate facility data acquisition system.

The IRIP test article is supported by an 80/20 aluminum frame. Contact between the IRIP and the frame was minimized and Teflon spacers were used to reduce heat leak between the IRIP and the frame.

Three surface thermocouples are located on the frame as shown in Figure 6 to help with heat leak calculations. The frame surface thermocouples are monitored by the IRIP data acquisition system. The test article was leveled to ensure an even distribution of water within the PCM section.

A schematic of the fluid loop, including instrumentation such as fluid temperature probes, pressure transducers, and pump, is shown in Figure 7. All fluid loop instruments are monitored by the IRIP data acquisition system.

The fluid loop is composed of an inner test loop, including Pump1, and an external conditioning loop including CH1. The standard configuration describes the system configured for fluid flow from right to left through the test article at nominal flow rates. The reverse configuration describes the

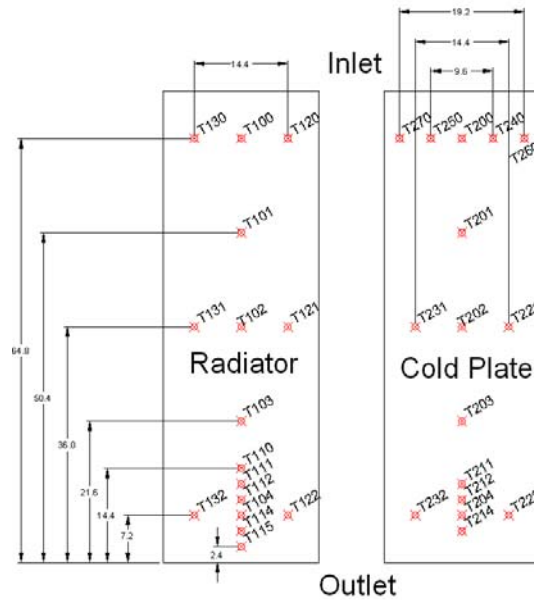


Figure 5. Test article surface thermocouple locations

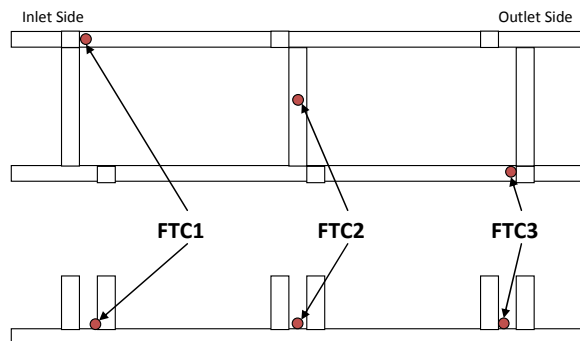


Figure 6. Thermocouple locations on support frame.

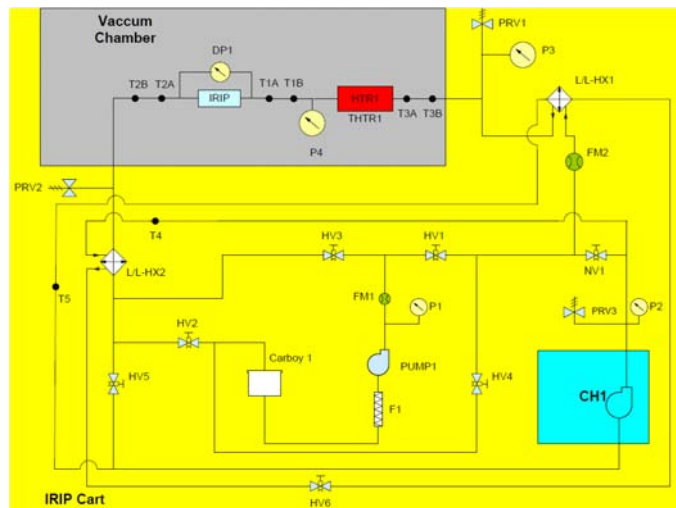


Figure 7. Fluid Loop instrumentation

system configured for fluid to flow through the test article from left to right at nominal flow rates. In both the standard and reverse configurations, the inner and outer loops are independent and isolated by HV5 and NV1. This changes in the Max flow configuration where Pump1 is not operated and CH1 provides sufficient head across NV1 to drive a higher than nominal flow rate in the design direction across the test article.

A. Test Parameters

A nominal heat load profile simulates the expected full scale heat load of a manned mission as described in Figure 8 such that approximately the same mass of ice remains at the end of the profile as at the start. The nominal heat rate profile is a superposition of the metabolic heat rate produced by crew members, the heat generated from avionics, and a heat load imposed by the environment such as solar heat introduced into the cabin through windows.

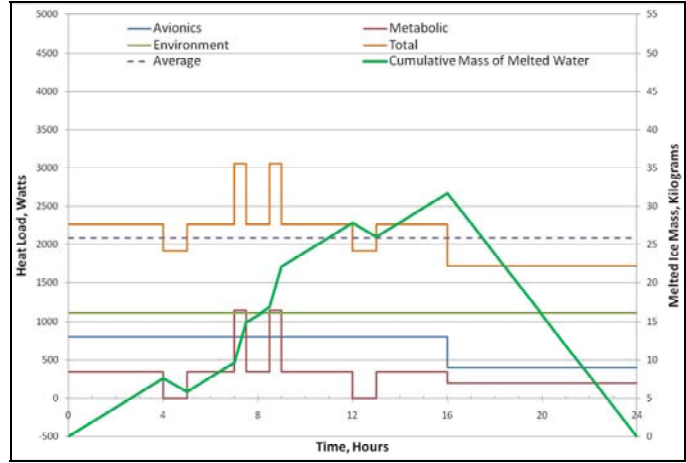


Figure 8. Full-size MMSEV heat load profile.

The IRIP presents approximately 0.15 times the surface area needed for the full scale design. In order to meet the condition that approximately the same mass of ice is present at start and completion of the heat profile, the heat rate is scaled according to the following equation

$$\frac{Q_c}{Q_{Fl}} = \frac{\dot{m}_c}{\dot{m}_{Fl}} = \left(\frac{\epsilon_c A_c (T_{ice}^4 - T_{LN2}^4)}{\epsilon_{Fl} A_{Fl} (T_{ice}^4 - T_{space}^4)} \right)$$

In order to best utilize test time the heat load profile is also accelerated through time-scaling. This effectively compresses the 24-hour heat load profile into a 12-hour heat load profile. The accelerated profile is determined by multiplying the time scale factor by the heat load delta above or below the average heat load. For example, a 12-hour heat load profile has a time scale factor of 2 (=24/12). With an average heat load of 2100 W, a point in the profile with a heat load of 2300 W has a delta of 200 W above the average. With a factor of 2, the delta of 200 W becomes 400 W, resulting in the original 2300 W being scaled up to 2500 W. This approach results in the same energy being put into or taken out of the PCM during each interval of the profile and maintains the same average heat load. The time scaled heat loads are implemented by adjusting the coolant flowrate to carry the heat delta while maintaining the profile coolant inlet temperature to the test article. A representation of the 12-hour accelerated IRIP heat load profile used during testing is shown in Figure 9.

A high heat load profile superimposes an additional constant heat load. This high heat load can be due to operation in a hotter than nominal environment. For this test an additional 300W are added to the scaled test article, the equivalent of an additional ~1800W on the full scale flight size.

III. TEST OPERATIONS

The order of the test conditions performed is shown in Table 1. A timeline of the major events during the testing is shown in Table 2.

The cyclical heat loads are evident in the plot of coolant inlet and outlet temperatures in Figure 10. The coolant inlet temperature follows the four nominal heat load profiles and two high heat load

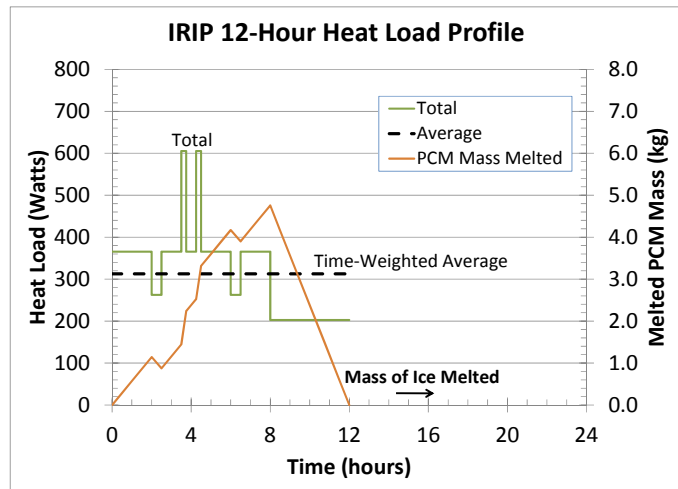


Figure 9. IRIP 12-hour heat load profile.

Table 1. Major Test Conditions.

Test Condition
High temperature (20°C) steady state
Pre-condition for Nominal heat load profile
Nominal heat load profile (~300W average heat load)
Low temperature (-10°C) steady state
High heat load profile #1 (~600W average heat load)
Pre-condition for High heat load
High heat load profile #2 (~600W average heat load)

temperatures are somewhat warmer than the sides and bottom since gravity keeps the bulk of the liquid nitrogen toward the bottom.

The heat lost by the coolant and rejected by the radiator is shown in Figure 12. The coolant heat loss (labeled on the plot as FluidPower) is calculated from the test data as $m_c \Delta T$, while the radiator heat rejection (labeled on the plot as RadiantPower) is calculated using the radiator surface and shroud temperatures. The four nominal heat load profiles and two high heat load profiles are obvious from the coolant heat loss plot, while the radiator heat rejection is much more constant.

During the four nominal heat load cycles, it can be seen that there are times where the applied heat load (the coolant

Table 2. Timeline of Major Events

Date & Time	Event Description
6/18/2012 7:52	Begin data acquisition. Begin toward high temperature steady state.
6/18/2012 19:22	Begin first test point of Nominal heat load profile.
6/20/2012 23:55	Begin toward low temperature steady state.
6/21/2012 5:12	Begin High heat load profile #1
6/21/2012 23:49	Begin pre-condition for High heat load #2.
6/22/2012 5:06	Begin High heat load profile #2.
6/22/2012 17:48	End High heat load profile #2 (loss of set point). Begin warm-up.
6/22/2012 18:21	Sudden rise of chamber pressure.
6/22/2012 23:33	End data acquisition.

radiator heat rejection, and ice is continually being melted. The phase front moves downstream toward the coolant outlet side until all of the ice is melted. This condition is referred to as “breakthrough” since the warm coolant temperature “breaks through” without being adequately cooled, and the system setpoint temperature control is lost.

The goal of the first test point, high temperature steady state, was to establish a steady state condition so that heat leak from the test article could be measured. If the test article was perfectly insulated, the heat lost by the coolant flowing through the IRIP would be equal to the heat rejection of the radiator surface. Without perfect insulation, any difference between the coolant heat loss and the radiator heat rejection at steady state is equal to the heat loss. This test point extends until the middle of the plot, until approximately 19:30

profiles, while the coolant outlet temperature is significantly damped out by the phase change material in the IRIP. Similar trends are also evident in the plots of surface temperatures shown in Figure 11.

After an initial cool-down period, the frame temperatures tend to follow the test article temperatures although with a more damped response due to the relatively good isolation between the two. Chamber shroud temperatures average about 100K. In general, the top shroud

temperatures are somewhat warmer than the sides and bottom since gravity keeps the bulk of the liquid nitrogen toward the bottom.

During the four nominal heat load cycles, it can be seen that there are times where the applied heat load (the coolant heat loss) is larger than the radiator heat rejection, and other times where the applied heat load is less than the radiator heat rejection. This is the nominal operation of the IRIP. The radiator is held at a fairly steady temperature, and therefore it radiates at a fairly steady heat rejection rate, while the applied heat load varies above and below the average. When the applied heat load is larger than the heat rejection, ice is being melted, and the phase front moves downstream toward the coolant outlet side. When the applied heat load is smaller than the heat rejection, water is being frozen, and the phase front moves upstream toward the coolant inlet side.

During the two high heat load cycles, the applied heat load is always larger than the

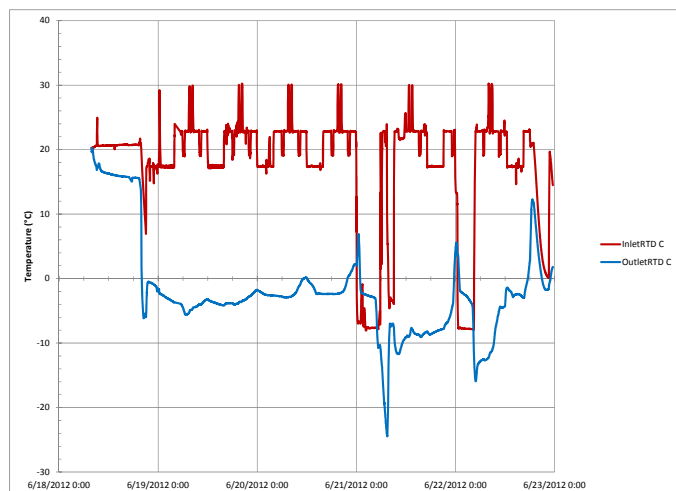


Figure 10. Coolant temperatures throughout entire test.

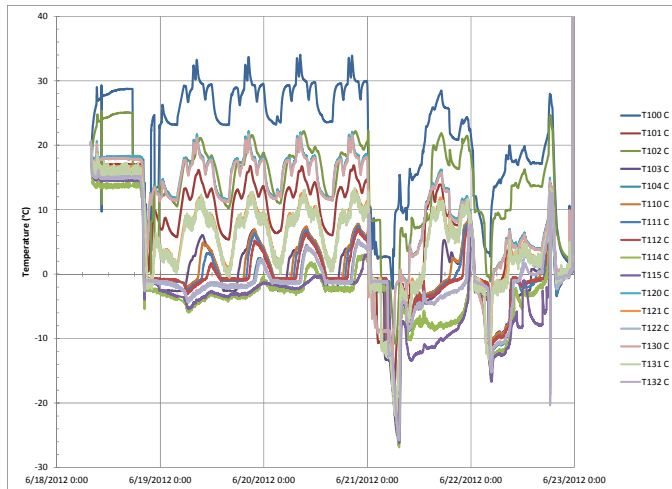


Figure 11. Top (radiator) surface temperatures throughout entire test.

The next portion of the test, the nominal heat load profiles, is meant to simulate a heat load profile that might be encountered by a vehicle such as the MMSEV. As explained in Section 0, a nominal 24-hour heat load profile is scaled to become a 12-hour test heat load profile due to the limited test time available. The magnitude of the overall profile is selected with the goal of having the average heat load equal to the average heat rejection of the radiator. Under these circumstances, there would be no net phase change over the heat load profile, and a vehicle such as the MMSEV could operate indefinitely under these design conditions.

The coolant inlet temperatures correspond to the applied heat load profile, while the coolant outlet temperature is nearly constant. In a thermal control system, the coolant exiting the IRIP would be mixed with coolant bypassing around the IRIP

to maintain the system setpoint temperature, which is assumed to be 1.7°C. In Figure 10 **Error! Reference source not found.** the coolant outlet temperature shows a slowly increasing trend, and eventually increases above the 1.7°C setpoint temperature, which would result in a loss of setpoint for the system. This indicates that the applied heat load profile was slightly greater than the design condition corresponding to the IRIP test article and the chamber environment. Possible explanations for this difference are addressed in Section 0. Likewise, the surface temperatures in Figure 11 show a similar trend. The warmer surface temperatures, which are located nearest the coolant inlet, appear to show a steady-repeating pattern. However, a closer examination of the cooler surface temperature near the outlet reveals that they are getting slightly warmer with each cycle. A slightly lower overall applied heat load profile would likely result in a steady-repeating condition that could have been repeated indefinitely.

Figure 12 shows a plot of the coolant heat loss and the radiator heat rejection during these four cycles. If the applied heat load and the radiator heat rejection were to perfectly balance each other, the red radiator heat rejection line would cut through the average of the blue applied heat load line. It appears visually from the plot that this is approximately the case, but the earlier plots indicate that the average of the applied heat load is slightly larger than the average of the radiator heat rejection.

As with the high temperature steady state condition that started the testing, a low temperature steady state condition was attempted so that heat leak from the test article could be measured at a second temperature. With heat leak measured at two different temperatures, a heat leak resistance value could be determined.

The coolant inlet and outlet temperatures for this test condition are shown in Figure 10. The previous heat load profile ends at approximately 6/21 00:00; the subsequent heat load profile begins at approximately 6/21 05:00. After the previous heat load profile was completed, the coolant inlet temperature was decreased to approximately -8°C, comfortably below 0°C in order to freeze all of the water PCM. The coolant outlet temperature remains closer to 0°C until all of the water PCM is frozen, at which time the coolant outlet temperature then drops below the inlet temperature. The surface temperatures are shown in Figure 11. For the most part, these surface temperatures decrease, then hold steady while water in the vicinity is freezing, and then decrease once again, in sequential order from inlet to outlet.

Error! Reference source not found. shows the coolant heat loss and the radiator heat rejection. The radiator heat rejection shows a slight

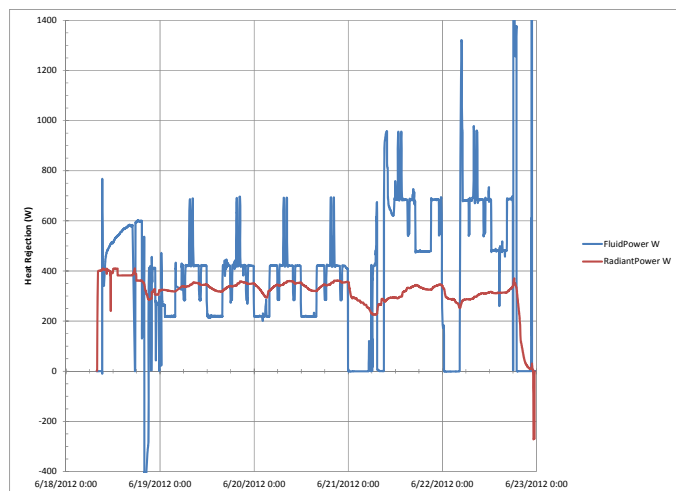


Figure 12. Heat rejection throughout entire test.

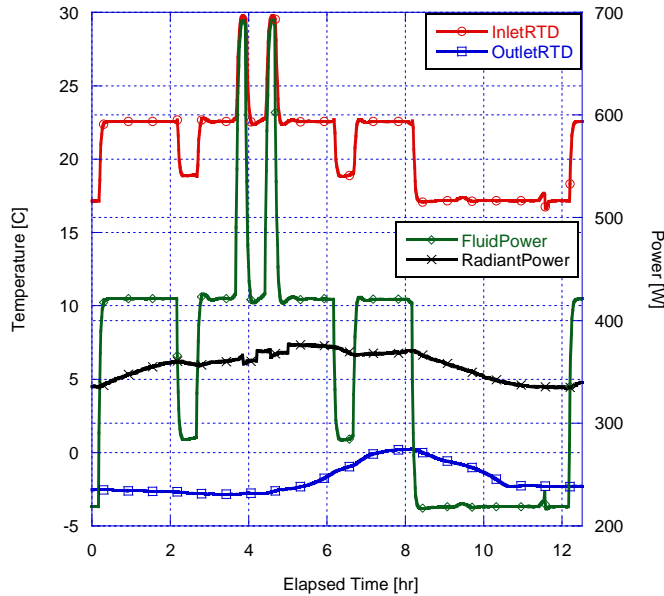


Figure 13. Test results from nominal heat load profile testing

to avoid coolant temperatures getting too cold, the flowrate was temporarily increased and then stepped down progressively until the coolant outlet temperature remained in a more acceptable range. After approximately 10:00, the high heat load profile progressed as planned. At approximately 00:00 on 6/22, the coolant outlet temperature rose above the assumed setpoint of 1.7°C, resulting in a loss of the simulated system setpoint. This was expected for this high heat load case, and before this condition was encountered, the IRIP provided adequate thermal control for multiple hours. The surface temperatures shown in Figure 11 tend to follow the shape of the applied heat load profile, although the temperatures closest to the outlet eventually increase when the system setpoint is lost.

Error! Reference source not found. shows how the overall applied heat load profile is larger than the heat rejection from the radiator. Since more heat is being applied to the water-ice than is being removed from it, net melting occurs during this test condition.

To prepare the test article for another high heat load case, the IRIP is completely frozen again as it was before the first high heat load case.

With the time remaining during the test, the same high heat load profile as before was run. Plots of the data in Figure 11 show trends similar to those observed in the previous case.

At approximately 18:00, the flowrate was increased to begin warming up the test article. At approximately 18:20, a loud bang was heard from the chamber, and chamber pressure rose suddenly. The chamber was actively repressurized beginning at approximately 18:30. After the chamber was repressurized and opened, a rupture in the radiator facesheet of the IRIP was observed. This failure was undesirable, but not completely unexpected. A fault tree for this failure is examined in Section 0.

downward trend due to the decreasing test article temperatures.

A high heat load profile was run next to demonstrate how the IRIP can provide thermal control and maintain setpoint for a limited time if the heat load is higher than the design heat load. The same situation would be encountered for a nominal heat load in an environment warmer than that for which the IRIP was designed. For example, an IRIP for the MMSEV designed for a lunar polar location could still provide thermal control for a shorter duration closer to the equator. The coolant inlet and outlet temperatures are shown in **Error! Reference source not found.** It is interesting to note that when the profile was first started a little before 06:00 on 6/21, even though the coolant inlet temperature was increased, the coolant outlet temperature continued to decrease. This occurred because the test article was still cold from the previous test condition, and because the coolant flowrate was decreased from what it had been previously, allowing a longer residence time for the coolant inside the cold test article. In order

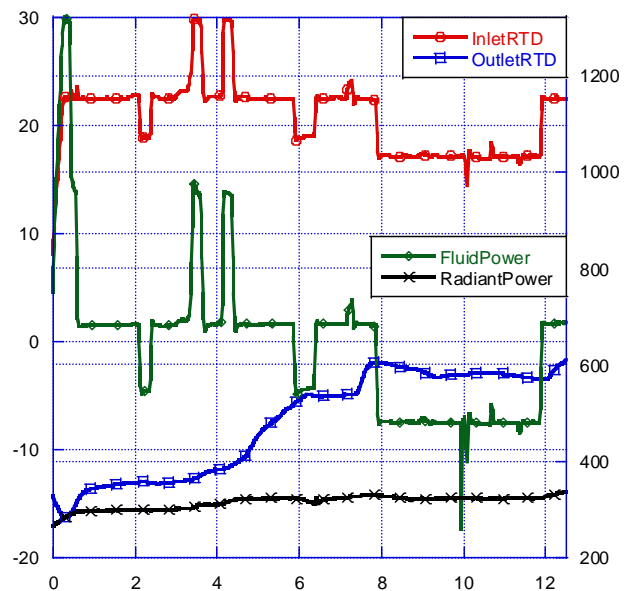


Figure 14. Test results from high heat load profile testing

TEST DATA

Data recorded during testing is very promising. Nominal tests indicate that the condition of no-net phase change was approached. Figure 13 shows an excerpt from the nominal profile testing. Note that though close, a slightly higher outlet temperature at the end of the cycle than at the beginning indicates some net decrease in the ice phase. A maximum outlet temperature of 0C indicates that the set point of 1.7C is always maintained and that design performance is near that predicted for this scale coupon.

High environment load tests, an example of which is shown in Figure 14, indicate the extent to which the IRIP can maintain setpoint for extended periods of time in extreme environments when

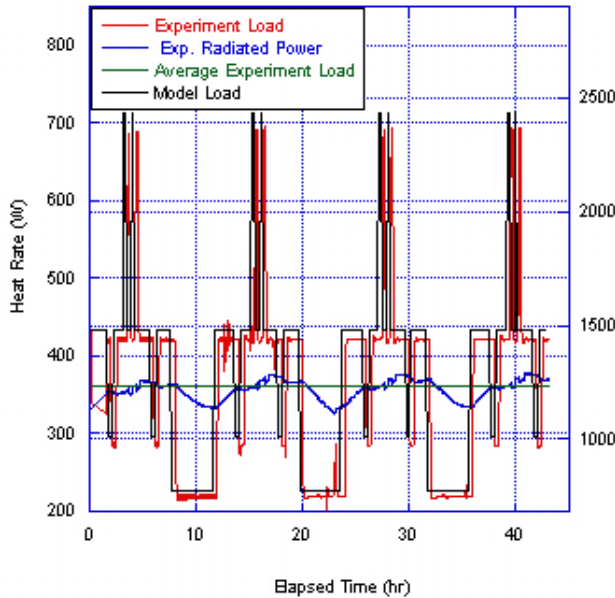


Figure 16. Experiment and model heat loads, including experiment average load and experiment radiated power.

design and the prediction of the behavior of this hardware. This model was used first to arrive at the geometry of a flight-like design then to scale this design geometry for a test article of a size appropriate for testing in Chamber E. The scale test article was then modeled with test conditions to predict test behavior, optimize test time, and identify pre-conditioning requirements needed for a successful test. These flight-like and scale test-article geometries are separate parametric cases of a single thermal desktop model that is shown in Figure 15.

This Thermal Desktop model is designed to produce the 2-D thermal behavior of an ideal integrated PCM radiator having a fluid loop as the heat source. The test hardware is designed to

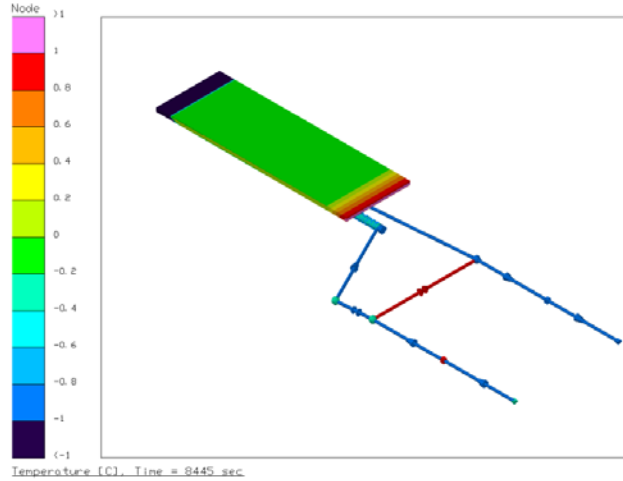


Figure 15. Thermal Desktop model

fully charged. The high heat load profile shown was pre-conditioned by fully freezing the PCM. Once frozen, the accelerated nominal profile, with an additional 327.5W load including a higher than nominal heat load applied during the first hour, was run until breakthrough, or loss of setpoint, was observed. Breakthrough occurred in both the case shown and a second case after approximately 13 hours. This corresponds to an accelerated 4280 W full scale load, twice the design load. Converted to a 24-hour profile, this is the energy equivalent of a 3190 W average load lasting 26 hours.

MODELING COMPARISON

A thermal desktop model was built to support the

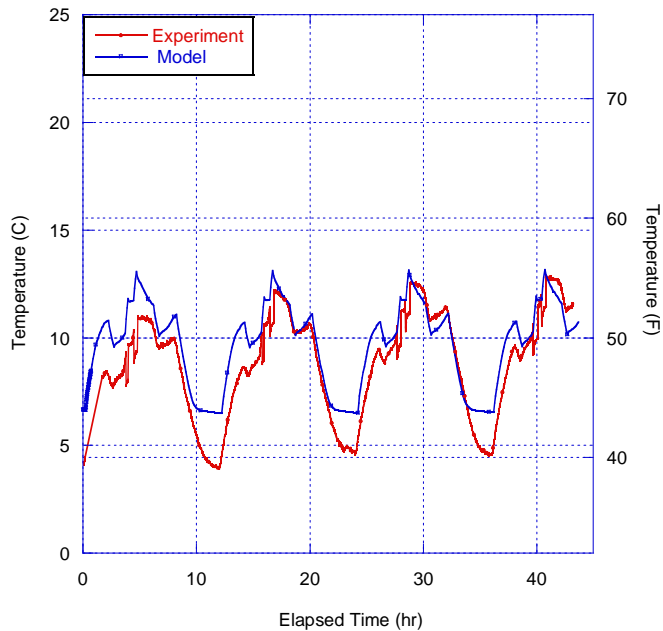


Figure 17 Average surface temperature of the experiment vs average surface temperature of the model

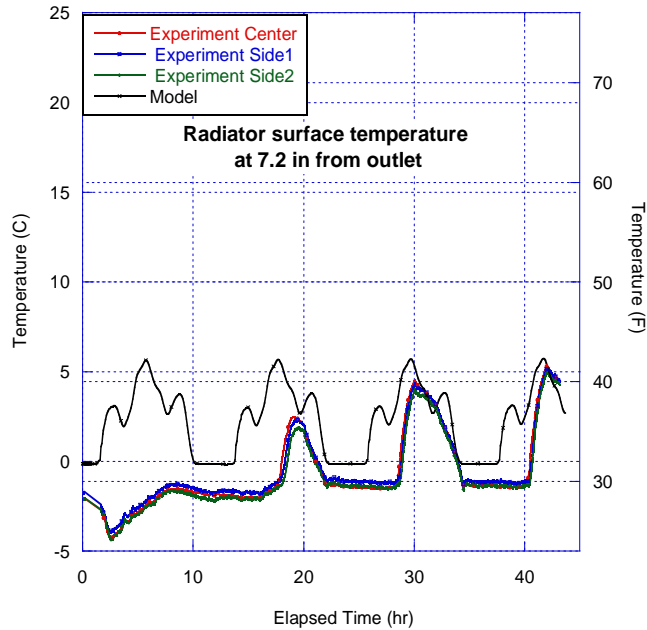


Figure 18 Temperature locations T104, T122, & T132 from the experiment vs the model

condition, i.e. the last bit of ice is consumed at the very moment that regeneration restarts. This design condition results in the minimum mass for the IRIP since it maximizes the average radiator temperature, which in turn minimizes the required radiator area. Another consequence of this design condition is that the device can operate indefinitely under a cyclic application of the design heat-load and never lose setpoint. If a mission requires a higher average heat load, the mission life is finite and a function of the starting ice content of the design, if a lower heat load is required, then excess heat rejected is stored in the PCM.

The test-article design is a scaled version of the flight-like design where the width of the device perpendicular to the direction of flow through the cold-plate is scaled to meet the limits of the test facility. Thus scaled the height and flow-length and, as a consequence, the temperature gradient along the flow-length of the test-article are identical to the flight-design. Flow rate and heat load profile are scaled by design width so that working fluid mass flux through the cold-plate and radiated heat flux remain unchanged from the flight-like design.

Comparisons of the experimental results with respect to the model predictions are presented in **Error! Reference source not found.** through **Error! Reference source not found.** **Error! Reference source not found.** shows experiment versus model heat loads. Experiment heat load is calculated as the sensible heat loss of the PGW thermal working fluid between the inlet and outlet of the cold-plate. A deviation of approximately 10W is apparent between the experiment and model heat loads. This difference is likely a consequence of the control scheme selected for the experiment – where the model applies a specific heat load, the experiment controls cold-plate inlet temperature and fluid flow rate to arrive at the desired heat load. The difference is on the order of 3% the desired average heat load and well within expectations. The

reproduce the predicted 2-D behavior by incorporating a mini-channel parallel flow finned cold-plate that spans the full width of the IRIP hardware with a specially designed header that ensures even distribution of flow through the cold-plate. This integrated cold-plate and the large extent of the hardware dimensions approximates the 2-D behavior one would expect in a theoretical infinite width design.

The flight-like design was developed based on the full-size MMSEV heat load profile, described in Figure 8. This is a 24-hour heat load profile that incorporates a constant environment load of 1100 W in addition to the expected metabolic and avionics loads over a 24-hour period. The mass of water PCM incorporated into the design is dictated by the mission requirement for radiation protection, 500 lbm. The radiator extent is sized to meet the average heat load of the 24-hour profile such that the cyclic minimum ice content in the heat profile of the hardware is constant and is at a minimum such that the outlet temperature, and thus system setpoint, never exceeds 1.7°C. This design condition is referred to as the “last-bit-o’-ice”

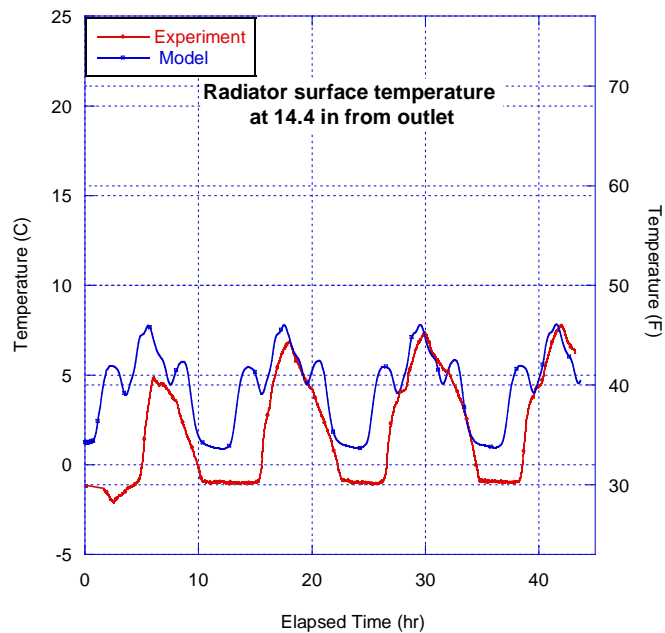


Figure 19 Temperature location T110 from the experiment vs the model

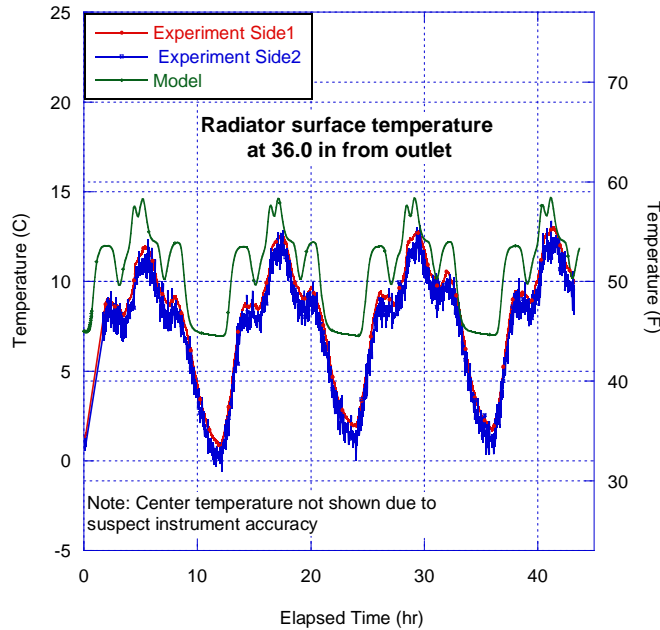


Figure 20 Temperature locations T131 and T121 from the experiment vs the Model

earlier with a low of 4.0 C and a high of 13.0 C. The average radiator surface temperature can be interpreted as reasonable indication of radiative heat rejection, and it appears from this comparison that the model predicts a higher radiation heat rejection than seen in experiment. There may be a few reasons for this, primary among these are assumptions in the model on interface conductances between components in the braze assembly and of the convective heat transfer coefficient in the cold-plate. Where these values are modeled higher than actual fact, the predicted surface temperature of the radiator will be nearer that of the fluid, so higher as seen here. Figure 18 through **Error! Reference source not found.** further compare radiator surface temperature between the model and experiment at specific instrument locations beginning near the cold-plate outlet and progressing to the inlet.

Figure 18 shows experiment and predicted temperatures at 7.2 in from the outlet, or instruments T104, T122, and T132. In this plot you can observe the progression of the ice front in the PCM toward the outlet as the cyclic peak temperature increases and the peak period widens. Eventually, at approximately 40 hours, the experimental peak is similar in magnitude and shape to the central peak of the model prediction. Note that the preceding and following predicted peaks are not seen in the experimental data – it appears that these are damped more substantially in the hardware than the model accounts for. Similar behavior is observed at 14.4 inches from the outlet, instrument location T110, seen in Figure 19 . Peak magnitude and shape are much as predicted, though intermediary peaks appear damped from the experiment. The intermediary peaks do become more apparent as we near the inlet, however, apparent in Figure 20. In Figure 20 the central peak splits into the two 30 minute heat load peaks, and gain still more definition in Figure 21.

Throughout these it appears that the experimental radiator surface temperature tends to be lower than

radiated power is shown in blue on this figure, and it varies in the vicinity of the average fluid heat load, shown in green. Experimental radiated power is calculated by discretizing the radiator surface area by instrument and summing the radiated heat between each instrument temperature measurement and the chamber shroud temperature. The average radiated power (not plotted in **Error! Reference source not found.**) is approximately 0.5% less than the average experiment heat load where the model predicts the two values as identical. This is close, though as a consequence after four cycles the experiment saw setpoint breakthrough where the goal was indefinite operation. A heat load reduced by 5W in the experiment would be sufficient to demonstrate indefinite operation of the integrated radiator design.

Figure 17 shows the average temperature of the radiator surface as measured in the experiment and as predicted by the model. The model shows a steady-state cyclic condition that repeats indefinitely from a low of 6.5 C to a high of 13.2 C. The experiment temperature rises steadily, though slowly, due to the slight addition of heat described

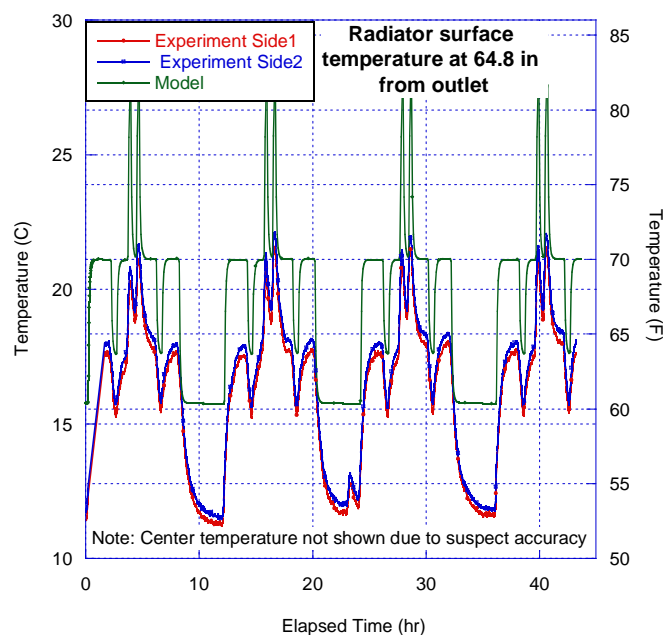


Figure 21 Temperatures from locations T130 and T120 of the experiment vs. the model

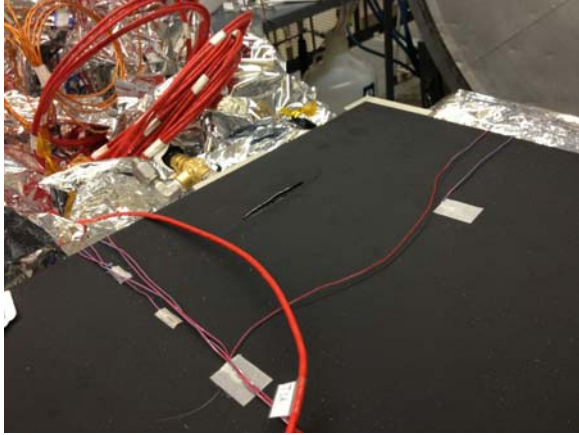


Figure 22. Facesheet tear

that predicted, suggesting higher resistance between working fluid and radiator surface than expected. The difference is at its greatest near the inlet, and though only a difference of about 3 C is seen between model and experiment at high points, the difference between the lowest temperatures is between 5 C and 8 C at all points upstream of the ice-front. The reason for this high versus low variation is not clear.

In general, the trends and behavior appear well predicted by the model with discrepancies that can be addressed to improve the prediction. A difference in heat rejection of about 3% is observed and experimental data indicates that a 0.5% lower heat rate would afford indefinite operation of the supported vehicle per the ‘last bit-o-ice’ design scenario.

RUPTURE FAILURE INVESTIGATION

Upon testing completion of IRIP and removal from vacuum chamber E, a 3.5 inch tear was discovered on the facesheet of the radiator surface (see Figure 22), thereby causing a failure in the test article. This tear extends parallel to the brazed fins and is nearest to the refrigerant exit of the cold plate.

While no single fault has been identified as the cause of the failure of the test article, two are believed more probable than others. These include ice buildup at unexpected locations due to water/ice trapped between the facesheet and fins and insufficient mechanical headroom. Insufficient mechanical and pressure headroom could have developed from directional freezing, uneven liquid distribution, or excess water in the test article. Evidence indicates that the test article was slightly overfilled which lends credence to this potential cause. Evidence through flash thermography also shows gaps between the facesheet and the fins into which water may be introduced through condensation during testing or sloshing during installation. Water penetrating these gaps would, though cyclical freezing, apply strong pressure loads which could have deteriorated the quality of the braze or caused yielding of the thin facesheet material.

SUMMARY AND CONCLUSIONS

IRIP is an integrated radiator and water phase change media heat rejection technology developed in support of the MMSEV project. In addition to its thermal control function, this technology provides protection for crewmembers within a vehicle from harmful radiation events and is a potential emergency source of potable water. The technology affords considerable flexibility for mission planning by affording the ability to operate for extended periods under heat loads that exceed the nominal heat rejection capacity of the radiator.

This technology was developed through thermal modeling based upon a nominal 24-hour flight-like heat load profile superimposed upon an assumed environment load. The IRIP test article hardware was fabricated as a scale version of the flight-like model design such that it replicates modeled thermal gradients, heat flux, and working fluid

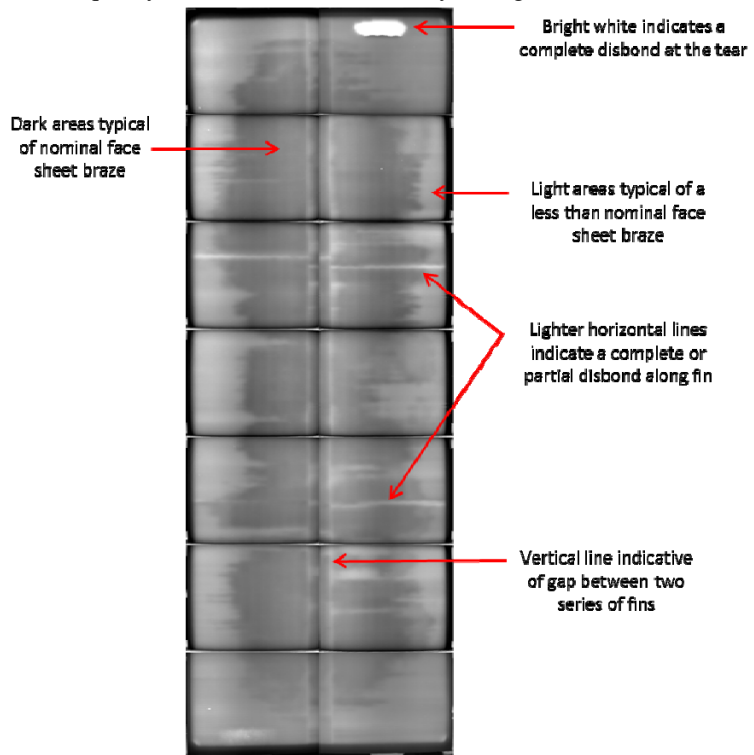


Figure 23. Thermography image (frame 49) indicating improper brazing

mass flux. All design dimensions and fabrication parameters were defined using the IRIP thermal model. Testing of the IRIP test article hardware demonstrated the technology's ability to maintain a nominal heat load for the mission equivalent of 96 hours operation before thermal control system setpoint breakthrough. Model predictions indicate that design optimization could raise radiator surface temperatures for improved heat rejection and thus result in indefinite vehicle mission operation time without thermal control system setpoint breakthrough. Testing further showed that the capacity of the integrated PCM affords considerable flexibility in mission planning such that when fully frozen the radiator is able to meet thermal control system needs at considerably elevated average heat loads. At the elevated heat loads tested, the hardware shows it is capable of operating at 150% the nominal heat load while still maintaining setpoint for up to 26 mission hours, or at 200% of the nominal heat load while maintaining setpoint for 13 hours. Comparing model predictions to experimental results shows a reasonable correlation with some room for improvement. Hardware radiator surface temperatures are slightly lower than those predicted so that test heat rejection is less than the heat load applied. As a result, where modeling indicates indefinite operation at the nominal heat load, testing demonstrated the equivalent of 96 hours mission time before breakthrough. Testing demonstrates that the IRIP design is a viable and flexible candidate for the thermal control of exploration vehicles. The next phase of development for this technology needs to address void control, PCM modes of failure, and quality control in manufacture of the hardware. These development needs are reinforced by a failure in the PCM section that occurred as hardware testing wrapped up on the final day. An analysis of this failure suggests most likely causes are associated with void control and flaws in the fin to facesheet braze joint. The IRIP heat rejection hardware is a promising and viable multi-function technology that can reduce radiator size, protect crewmembers from radiation events, and improve mission flexibility for multi-mission vehicles intended for exploration.

REFERENCES

- Lee, Steve, "REDU Thermal-Vacuum Test Report," CTSD-ADV-742, September 15, 2009.
- Lee, Steve A., Leimkuehler, Thomas O., Stephan, Ryan, and Le, Hung V. "Thermal Vacuum Test of Ice as a Phase Change Material Integrated with a Radiator," AIAA-2010-6113.
- Cognata, Thomas J., "Rover Heat Sink (RoHS) Experimental Report and Analysis," CTSD-ADV-894, February 4, 2011.
- Cognata, Thomas J., Leimkuehler, Thomas O., Balasubramaniam, R., Nayagam, Vedha, Hasan, Mohammad, and Stephan, Ryan, "A Review of the Experimental and Modeling Development of a Water Phase Change Heat Exchanger for Future Exploration Support Vehicles," AIAA-2011-5208.
- Leimkuehler, T. O., Government Fiscal Year 2011 Replicative Ice PCM (RIP) Test Report, CTSD-ADV-957, September 30, 2012
- Leimkuehler, T. O., Replicative Ice PCM (RIP) Test Report, CTSD-ADV-849, December 10, 2010.
- Hansen, S. Replicative Ice PCM (RIP) Test Report, CTSD-ADV-745, September 30, 2009.
- Leimkuehler, T. O., Stephan, R. A., and Hansen, S., "Development, Testing, and Failure Mechanisms of a Replicative Ice Phase Change Material Heat Exchanger," AIAA-2010-6138, 40th International Conference on Environmental Systems (ICES), Barcelona, Spain, July 2010.
- Leimkuehler, T. O., Stephan, R. A., and Hawkins-Reynolds, E., "Testing and Failure Mechanisms of Ice Phase Change Material Heat Exchangers," AIAA-2011-5207, 41st International Conference on Environmental Systems (ICES), Portland, Oregon, July 2011.
- Leimkuehler, T. O., and Stephan, R. A., "Experimental Investigation of Phase Change Material Heat Exchangers," AIAA-2012-3520, 42nd International Conference on Environmental Systems (ICES), San Diego, California, July 2012.